Robotica (2014) volume 32, pp. 1363–1382. © Cambridge University Press 2014
doi:10.1017/S0263574714001957

ASSISTON-FINGER: **An under-actuated finger exoskeleton for robot-assisted tendon therapy**

Ismail Hakan Ertas, Elif Hocaoglu and Volkan Patoglu*

Faculty of Engineering and Natural Sciences, Sabancı University, 34956 Istanbul, Turkey
{hertas,elifhocaoglu}@sabanciuniv.edu

(Accepted June 20, 2014. First published online: July 17, 2014)

SUMMARY

We present ASSISTON-FINGER, a novel under-actuated active exoskeleton for robot-assisted tendon therapy of human fingers. The primary use for the exoskeleton is to assist flexion/extension motions of a finger within its full range, while decreasing voluntary muscle contractions helping to keep the tendon tension levels to stay within acceptable limits, avoiding gap formation or rupture of the suture. The device can also be employed to administer range of motion (RoM)/strengthening exercises. ASSISTON-FINGER is designed to be passively back-driveable, can cover the whole RoM of patients, and can do so in a natural and coordinated manner. In particular, the device employs human finger as an integral part of its kinematics and when coupled to a human operator, the parallel kinematic structure of exoskeleton supports three independent degrees of freedom, dictated by the kinematics of the human finger. Automatically aligning its joint axes to match finger joint axes, ASSISTON-FINGER can guarantee ergonomy and comfort throughout the therapy. The self-aligning feature also significantly shortens the setup time required to attach the patient to the exoskeleton. We present the kinematic type selection for the exoskeleton to satisfy the design requirements for tendon therapy applications, detail optimal dimensional synthesis of the device considering trade-offs between multiple design criteria and discuss implementation details of the exoskeleton. We also present feasibility studies conducted on healthy volunteers and provide statistical evidence on the efficacy of exoskeleton driven exercises in keeping the average muscle recruitment and the maximum tendon tension levels as low as human guided therapies.

KEYWORDS: Finger exoskeleton; Tendon therapy; Rehabilitation; Design optimization; Dimensional synthesis; Under-actuation.

1. Introduction

More than one million people in the world receive treatment in emergency departments annually, due to acute hand and finger injuries. Tendon injuries are one of the most frequent problems encountered among these injuries.[1] The loss of hand function is a major source of disability that prevents patients from performing activities of daily living and significantly limits their employment opportunities.

Most tendon injuries require surgical repair of damaged tendons with the goal of restoring the normal function of joints and their surrounding tissue. After a tendon repair surgery, healing may take couple of weeks, during which the injured finger is immobilized in a splint. Unfortunately, healing of scar tissue causes adhesion of the tendons, the tendon sheath and the surrounding tissue, limiting the motion of the finger after the repair. The most common and disturbing problem that patients experience after a tendon injury is finger stiffness, that is, inability to either fully bend (flexor tendon injury) or straighten the finger (extensor tendon injury). Avoiding finger stiffness requires complete recovery of tendon excursion so that the full range of motion (RoM) of the finger is regained.

Adhesion of the tendon can be avoided if an appropriate early hand rehabilitation protocol is followed to enforce gliding of the tendon.[2] Hence, while treating tendon injuries, it is of utmost importance to ensure the right balance between postoperative immobilization of the finger to allow

* Corresponding author. E-mail: vpatoglu@sabanciuniv.edu

healing and early mobilization of the finger to avoid adhesion formation and improve strength of the repair site.[3,4] Interim period finger rehabilitation exercises include pinching to promote isolated tendon gliding,[5,6] while late period patients are asked to perform resistance exercises to ensure strength.[7,8]

1.1. Tendon therapy

In the literature,[4,9,10] early mobilization of the finger, starting within a few days of repair, is advocated. In particular, early mobilization techniques are claimed not only to inhibit adhesion formation but also to promote intrinsic healing, producing a stronger repair site than possible with immobilization.[2]

Early mobilization can be exercised when the injured finger movement is active or passive. *Active* mobilization techniques require patients to perform voluntary flexion and extension exercises, but this form of rehabilitation is risky, since inappropriate amount of stress induced on the tendon by the voluntary muscle contractions may cause gap formation or rupture of the repair site.[11]

There exists two commonly used *passive* early mobilization techniques: the modified Duran technique and the Kleinert method. In the modified Duran technique, a therapist enforces coordinated motions to the injured finger within closely controlled joint limits, while the patient stays relaxed throughout the therapy.[9] Due to extensive involvement of the therapist in the modified Duran technique, this therapy has relatively high treatment cost. Moreover, therapist induced trajectories lack repeatability and quantitative measurements of patient progress. The Kleinert method utilizes a dynamic splint that attaches the proximal phalanx of the finger to the wrist with a rubber-band and constrains the wrist movements. For flexor (extensor) tendon injuries, the rubber band applies forces to aid flexion (extension) of the finger. The Kleinert method combines active and passive movements of the finger such that the patient stays passive while flexing (extending) the injured finger; the patient is active during extension (flexion) of the finger.[5,6,12] Unfortunately, the Kleinert method cannot provide coordinated motion to the injured finger due to the simple structure of the dynamic splint.

1.2. Rehabilitation devices for tendon injury

Conventionally, physical rehabilitation after a tendon injury is performed in hospitals, using intense hand training, electro-stimulation or drug treatment. Robot-assisted rehabilitation therapies help eliminate the physical burden of therapy for the therapists, and enable cheap, safe and versatile training with increased intensity and accuracy. These devices are also advantageous, as they can provide quantitative measurements of patient progress. Clinical trials on robot assisted rehabilitation provide evidence that this form of therapy is effective and possesses high potential.[13–16]

The most common devices used to aid the recovery of joints immediately after trauma or surgery are simple non-actuated devices, such as Thera-Band[17] and Digiflex.[18] These devices help with the opening/closing of the hand or flexion/extension of fingers. Continuous passive motion (CPM) is another therapy method utilized to assist motion of hand. CPM devices, such as Kinetec 8091 Portable Hand CPM[19] and Amedeo system[20] constantly move the joint through a controlled RoM, where RoM is determined by the therapist. In addition to these simple devices, various finger/hand exoskeleton devices have been developed for rehabilitation of finger/hand function.[21–25] However, most of these devices are designed to target treatment of stroke patients. Devices proposed for stroke therapy may not be appropriate for administration of tendon therapy exercises, since these devices are designed for high torque outputs and lack the desired level of back-driveability required for tendon therapy. Furthermore, some of these devices are based on restricting joint motions,[26,27] while some others can only exert forces along a single direction.[28]

The design of a finger exoskeleton and the administration of tendon therapies need to be handled carefully, as the challenges involved in robot assisted tendon therapy exercises are significantly different than other robot assisted therapies. There exits several devices that are designed for tendon therapies.[29–32] In particular, in ref. [30], an end effector type device is proposed for hand injuries. Since this device can exert forces only at the finger tip, it cannot ensure coordinated motion of the fingers as required for the tendon therapies. The devices proposed in ref. [29] and [31, 32] are fully-actuated tendon based devices. They require many actuators to be employed; hence, are complex, expensive, and hard to control.

In this paper, we propose an under-actuated exoskeleton for finger rehabilitation that is specifically designed for the tendon repair therapies. ASSISTON-FINGER can assist the finger motion within its full range in a natural and coordinated manner, while providing quantitative measurements of finger

Table I. Means and standard deviations of joint angle (RoM) measurements (in degrees) for four fingers.[35]

Finger	MCP (°)	PIP (°)	DIP (°)
Index	70.83 (11.09)	103.87 (7.79)	61.17 (12.71)
Middle	85.30 (9.87)	103.98 (8.98)	73.64 (16.30)
Ring	85.09 (14.46)	107.15 (13.49)	66.96 (15.77)
Pinky	85.58 (18.09)	98.95 (11.20)	70.79 (15.84)

movements and actuator torque. Enabling passive exercises, ASSISTON-FINGER can significantly decrease voluntary muscle contractions, helping keep the tendon tensions within acceptable limits to avoid gap formation or rupture of the suture. Preliminary results for this design have been presented in IEEE ICORR.[33] This paper significantly extends the conference version by detailing the design requirements for tendon therapy, introducing optimal dimensional synthesis, discussing implementation details and providing extended results.

The paper is organized as follows: Section 2 introduces the kinematic model of human finger and overviews the design requirements for a finger exoskeleton to be employed for tendon repair therapy exercises. Section 3 presents the kinematic type selection of the device. Optimal dimensional synthesis is detailed in Section 4. Implementation details and operation modes of the finger rehabilitation system are explained in Sections 5 and 6, respectively. Human subject experiments for user evaluations are presented in Section 7, while empirical evidence on the efficacy of the device is provided and discussed in Section 8. Finally, Section 9 concludes the paper.

2. Human Finger and Design Requirements

Biomechanics literature suggests that the human finger (except the thumb) can be modeled as a serial URR[1] manipulator with four degrees of freedom (DoF). From the distal end, the joints are named as distal interphalangeal (DIP), proximal interphalangeal (PIP), and metacarpophalangeal (MCP), respectively. The DIP and PIP joints have flexion/extension DoF, while the MCP joint has both flexion/extension and abduction/adduction DoF. The distance between these joints depends on person's gender, age and other characteristics.

Exoskeletons are attached to human limb at multiple interaction points and movement of these devices correspond with human joints. An imperative design criteria while developing an exoskeleton-type rehabilitation robots is conforming with the underlying kinematics of the human joints and ensuring ergonomic exercises throughout the workspace. For instance, during the coordinated movement of a human finger, an ergonomic finger exoskeleton must ensure alignment of robot joint axes with finger joint axes. Misalignment of joint axes is highly detrimental as it results in parasitic forces on the patient around the attachment points and at the joints, causing discomfort or pain, or even long term injury under repetitive use. Most importantly, axis misalignment may promote compensatory movements of patients that can inhibit potential recovery and decrease real life use of the limb due to unfavored energetics of these movements.[34]

A finger exoskeleton appropriate for treatment of tendon injuries is required to cover the natural RoM for the flexion/extension motion of each finger joint. Table I presents the mean and standard deviation of the maximum observed RoM of MCP, PIP, and DIP joints of each finger. In ref. [35], the data presented in this table was collected over 15 human subjects, with a broad distribution of age and sex. Subjects were asked to maximally flex and extend each of their joints in all four fingers, one joint and finger at a time and the maximum RoM were determined using a video image analyzer. According to Table I, the mechanism must attain at least three DoF. Ergonomics not only necessitates the collocation of finger and device joint axes, but also requires that the kinematics of the exoskeleton support the natural finger motions without any interference throughout the whole motion range.

Another design criteria for an exoskeleton is ability for the device to accommodate a large range of population. Table II presents anthropomorphic data for nominal finger knuckle lengths as listed in.[36] Moreover, appropriate amount of torque needs to be generated by the robot at each joint to overcome inherent resistance at patients' digits. Hence, the minimum torque transmitted to each joint must

[1] Symbols U and R stand for universal and revolute joints, respectively.

https://doi.org/10.1017/S0263574714001957 Published online by Cambridge University Press

Table II. Means and standard deviations of human finger lengths (in mm) for four fingers.[36]

Finger	$L_{proximal}$ (mm)	L_{middle} (mm)	L_{distal} (mm)
Index	39.78 ± 4.94	22.38 ± 2.51	15.82 ± 2.26
Middle	44.63 ± 3.81	26.33 ± 3.00	17.40 ± 1.85
Ring	41.37 ± 3.87	25.65 ± 3.29	17.30 ± 2.22
Little	32.74 ± 2.77	18.11 ± 2.54	15.96 ± 2.45

Table III. Finger Joint Activation Torques.

Torques	PIP abd/add	PIP flex/ext	MCP flex/ext	DIP flex/ext	Unit
Joint activation[37]	170	290	290	200	(N-mm)
Worst case gliding[38,39]	n/a	11.1 ± 1.6	6.2 ± 0.9	4.5 ± 0.7	(N-mm)

satisfy minimum required activation torque of that joint. Table III presents the required actuation torque for each finger joint according to,[37] while also reporting the torque required at each joint to overcome the peak gliding resistance of a Locking Lee Suture according to a worst case analysis.[38,39]

We have conducted survey with engineers and health professionals to help determine the design requirements for a finger rehabilitation robot.[40] According to this study, in addition to the anatomical and physiological requirements, there exist some psychological and mechanical requirements that a rehabilitation robot must satisfy. The most important of these requirements is that the robot must be safe, even under power losses. For a tendon rehabilitation device, this requirement dictates the need for the robot to be passively back-driveable, in addition to inclusion of software limits implemented through controllers. Passive back-driveability ensures safe interaction with the device when all actuators are disabled and guarantees safety even under controller errors.

Furthermore, since many of the targeted patient population are expected to have edema in their hands, the interaction points of the robot must be soft and comfortable, not cause physical injury or pain to the patient. Ease of attachment/detachment and ability to fit different finger sizes without necessitating time consuming manual adjustments are other consideration that are important for comfort. Finally, the robot must be compact and aesthetically pleasing in order to not overwhelm patients who might not interacted with a robotic rehabilitation device before.

3. Kinematic Type Selection

In order to span the whole natural flexion/extension RoM of a human finger and to do so robustly for various operators with different finger dimensions, a parallel mechanism based kinematic structure is adapted for ASSISTON-FINGER, for which the kinematics of the human finger is an integral part of the device kinematics. The device is only operational when worn by a human operator. When coupled to the human operator, the parallel kinematic structure of exoskeleton supports three independent DoF, dictated by the kinematics of the human finger. Hence, the device not only can cover the whole RoM of any operator, but it can also do in a completely ergonomic manner. Automatically aligning its joint axes to match finger joint axes, ASSISTON-FINGER can guarantee comfort throughout the therapy. The self-aligning feature also significantly shortens the setup time required to attach the patient to the exoskeleton. Moreover, the linkage based kinematic structure of the parallel mechanism is advantageous over cable driven transmission mechanisms, since linkages allow for direct and efficient transfer of forces from the grounded actuator to each phalanx of the finger.

Having three DoF, up to three independent actuators can be utilized to control the mechanism. However, for physical therapy exercises following tendon injuries, independent motion of each phalanx of the finger is hardly necessary, as long as a wide range of coordinated finger motions can be supported and the whole RoM of the finger is covered. Hence, an under-actuated mechanism is selected for the kinematic structure of ASSISTON-FINGER. The choice of an under-actuated mechanism is also advantageous as it embodies further ergonomy and safety into the design. In particular, the uncontrolled DoF of the device can passively compensate for the alignments errors between the joint axes of the finger and the exoskeleton. In addition to the utilization of adjustable linkages and

https://doi.org/10.1017/S0263574714001957 Published online by Cambridge University Press

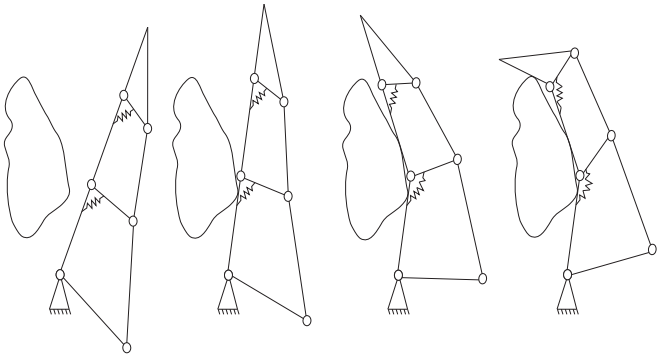

Fig. 1. Schematic representation of the motion of the under-actuated parallel kinematic chain against an obstacle.

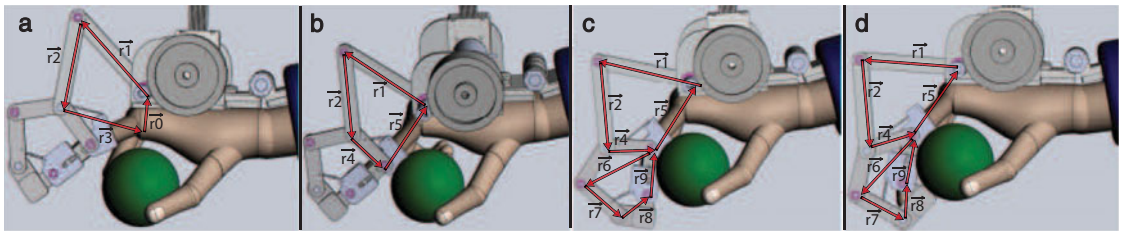

Fig. 2. (Colour online) Kinematic constraint loops indicating motion of each finger joints for (a) MCP, (b) PIP and (c) DIP.

connectors to ensure that the center of rotation of the human joints are aligned with the device axis, the inherent passive compensation adds further robustness into the device. Furthermore, under-actuation enables size, weight, and cost reduction for the exoskeleton, since the actuators are typically the largest, heaviest and most expensive components of the device.

Figure 1 depicts a schematic representation of the kinematic structure used for ASSISTON-FINGER, while Figs. 1 and 2 present the motion of the device against an obstacle. The kinematics of the exoskeleton is similar to the under-actuated fingers introduced by Gosselin *et al.* [41] and is effectively equivalent to the kinematics of a series of four/six-bar mechanisms that are coupled to each other with compliant springs and constrained by mechanical joint limits. Compliant springs are used for the mechanism to ensure a coordinated motion of the phalanges. In particular, the springs maintain the second and third phalanges of the finger in fully extended configurations until the first phalanx comes in contact with an obstacle or reaches a mechanical limit. When the mechanism is free of contacts and within joint limits, it behaves like a single rigid body. But when the motion of a phalanx is resisted, the torque generated by the motor overcomes the spring pre-load and the adjacent phalanx initiates motion. The motion continues sequentially until movements of all phalanges are resisted, due to either contacting with an object or reaching to the joint limits. Hence, the mechanism is capable of reproducing many of the natural finger trajectories and the actuator forces are distributed over all phalanges. The spring pre-load at each joint can be customized to accommodate patients with different finger stiffness levels.

During therapy, the motion of the under-actuated mechanism complies with the natural grasping motions of the finger and motion can easily be modulated to target different exercises through the introduction of custom joint limits, spring pre-loads, or obstacles. Hence, ASSISTON-FINGER is appropriate to target RoM and strengthening exercises. During flexion, the motion starts around the MCP joint until the first phalanx encounters an obstacle or the MCP joint limit is achieved. When the motion around the MCP joint is resisted, the force threshold dictated by the compliant spring between first and second phalanx is overcome and motion around the PIP joint initiates. Once again if the motion around the PIP joint is resisted due to an obstacle or joint limit, then the force threshold of the second compliant spring is exceeded and the third phalanx moves about the DIP joint. During extension, the movements take place in the reverse order until joint limits of DIP, PIP, and MCP are reached, sequentially.

https://doi.org/10.1017/S0263574714001957 Published online by Cambridge University Press

ASSISTON-FINGER has a linkage based planar kinematic structure that is formed by a series of four bar structures. The motion of each joint is ensured through different four bars. MCP joint can cover its RoM satisfying the vector loop equation

$$\overrightarrow{r_0} + \overrightarrow{r_1} + \overrightarrow{r_2} + \overrightarrow{r_3} = \overrightarrow{0} \tag{1}$$

as shown in Fig. 2(a). When the first knuckle completes its motion, the second knuckle rotates around PIP joint in all its motion range under the constraint of the vector loop equation

$$\overrightarrow{r_1} + \overrightarrow{r_2} + \overrightarrow{r_4} + \overrightarrow{r_5} = \overrightarrow{0} \tag{2}$$

as depicted in Fig. 2(b). Finally the third knuckle turns around DIP joint with the kinematic constraint

$$\overrightarrow{r_1} + \overrightarrow{r_2} + \overrightarrow{r_4} + \overrightarrow{r_5} = \overrightarrow{0} \tag{3}$$

coupled with

$$\overrightarrow{r_6} + \overrightarrow{r_7} + \overrightarrow{r_8} + \overrightarrow{r_9} = \overrightarrow{0} \tag{4}$$

as marked in Figs. 2(c) and 2(d).

4. Optimal Dimensional Synthesis

Our preliminary designs[33] revealed that the performance of ASSISTON-FINGER is highly sensitive to its dimensions and optimization studies are absolutely necessary for the proper design of the exoskeleton.

In the literature, several optimization studies have been conducted for finger devices. Cabas *et al.* optimized a robotic hand with three under-actuated fingers to increase its manipulation capability.[42] Nacy *et al.* optimized grasp stability of a three phalanx under-actuated prosthesis finger.[43] Wu *et al.* performed an optimization study for increasing the efficiency of object adaptation for a finger with a single active DoF.[44] In ref. [45], a multi-objective optimization is performed for an under-actuated finger to maximize its transmission efficiency and grasp stability. Similarly, Birglen and Gosselin optimized a two phalanx under-actuated finger to have force isotropy and grasp stability.[46]

However, all of these optimization studies have been performed for design of prosthetic fingers and in order to obtain force isotropy and/or grasp stability by varying the knuckle lengths in the design. Yet, exoskeleton type finger devices cannot be optimized in this way, since knuckle lengths are not design variables, but are dictated by the user. Furthermore, the performance metrics for rehabilitation devices are fundamentally different from those of prosthetic devices.

4.1. Problem definition

The performance requirements to be optimized are determined based on the targeted use scenario for the device. For a tendon therapy device, its important for the exoskeleton to be transparent in order to display minimal parasitic dynamics, while simultaneously being capable of delivering the required torque levels to mobilize each joint throughout its RoM. Along these lines, two objective functions characterizing the kinematic and dynamic performance of the mechanism are considered for optimal dimensional synthesis of ASSISTON-FINGER. In particular, the worst-case torque transmission of the exoskeleton is maximized, while its apparent inertia is minimized over a predetermined workspace.

The worst-case torque transmission is calculated by a workspace search for the maximum of minimum torques at the finger joints. Defining τ_{act} and τ_{end} as the actuator and end effector torques, respectively and letting J denote the kinematic Jacobian

$$\tau_{end}(q_1, q_2, q_3) = J^{-T}(q_1, q_2, q_3)\, \tau_{act}. \tag{5}$$

https://doi.org/10.1017/S0263574714001957 Published online by Cambridge University Press

the first objective function can be defined as

$$F_1 = \max_{q_1 \in W_1, q_2 \in W_2, q_3 \in W_3} \min \tau_{end}(q_1, q_2, q_3) \tag{6}$$

where q_1, q_2, q_3 are the angular positions and W_1, W_2, W_3 are the workspaces of MCP, PIP and DIP joints of finger, respectively. Since τ_{act} is kept constant, this objective function is directly proportional to $J^{-T}(q_1, q_2, q_3)$.

The worst-case apparent inertia is calculated as the minimum of maximum apparent inertia of device throughout its workspace. Defining M as mass matrix of the robot and the apparent inertia I reads as

$$I(q_1, q_2, q_3) = J^{-T}(q_1, q_2, q_3)\, M\, J^{-1}(q_1, q_2, q_3). \tag{7}$$

Accordingly, the second objective function is defined as

$$F_2 = \min_{q_1 \in W_1, q_2 \in W_2, q_3 \in W_3} \max I(q_1, q_2, q_3) \tag{8}$$

where the objective function matrix F can be expressed as

$$F = [-F_1 \quad F_2]^T. \tag{9}$$

Several constraints are imposed during optimization to ensure the proper direction of motion, to satisfy the geometric requirements to form four-bar mechanisms over the whole workspace and to prevent self-collisions.

The first constraint ensures that while actuated link is rotating in one direction, the finger knuckles also rotate in the same direction. More formally, the sign of the angular velocity of actuated linkage and the finger joints must be the same, that is, kinematic Jacobian must assume positive values throughout the whole workspace. Accordingly, the first constraint reads as

$$G_1 = -J(q_1, q_2, q_3) \quad \forall \quad q_1 \in W_1, \quad q_2 \in W_2, \quad q_3 \in W_3 \tag{10}$$

The second constraint states that the chosen link lengths must satisfy the four-bar construction criteria within their whole workspace, that is, the largest link length must be smaller than the total link length of all other links forming the four-bar mechanism. This constraint can be formally expressed for a four-bar mechanism with link lengths l_a, l_b, l_c and l_d as follows

$$G_2 = 2\, max([l_a, l_b, l_c, l_d]) - (l_a + l_b + l_c + l_d) \quad \text{for all fourbars} \tag{11}$$

The second constraint must hold for all the four-bar linkages depicted in Fig. 2 and defined by Eqns. (1)–(4).

The third constraint prevents self-collisions during the motion of finger exoskeleton. There are two possible collisions that require precaution: the actuated link can collide with the actuator or with the base platform of the robot. These two collisions may occur at the boundaries of the workspace; hence, a collision check is added at the both ends of the workspace. From the geometry of the system, the angle of the actuated link $r_{1_{angle}}$ is limited to stay within the range of $[-80^\circ \quad 140^\circ]$ throughout the whole finger movements. Formally, the third constraint reads as

$$G_3 = \begin{pmatrix} r_{1_{angle}} - 140 \\ -r_{1_{angle}} - 80 \end{pmatrix} \tag{12}$$

Consequently, the constraint matrix G can be stated as

$$G = [G_1 \quad G_2 \quad G_3]^T \tag{13}$$

https://doi.org/10.1017/S0263574714001957 Published online by Cambridge University Press

Table IV. Definition of the design variables.

D.V.	Var.	Definition	Range
α_1	L_1	Length of first link	50–120 (mm)
α_2	L_2	Length of second link	50–120 (mm)
α_3	L_{31}	Length of first part of third link	30–60 (mm)
α_4	L_{32}	Length of second part of third link	0–60 (mm)
α_5	L_4	Length of fourth link	20–70 (mm)
α_6	γ_3	Angle of third link	0–180 (°)

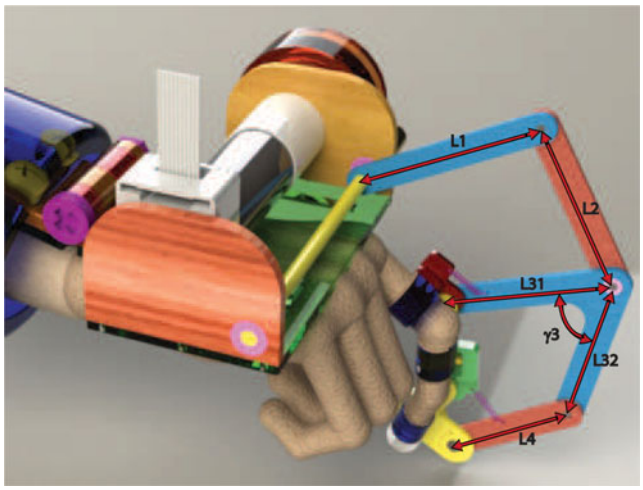

Fig. 3. (Colour online) Design variables are depicted on a solid model of the mechanism.

while the negative null form of the multi-objective optimization problem can be expressed as

$$\begin{aligned} min \quad & F(\alpha, \beta, \gamma) \\ & G(\alpha, \beta) \leq 0 \\ & \alpha_l \leq \alpha \leq \alpha_u \end{aligned} \tag{14}$$

where F represents the column matrix of objective functions that depend on the design variables α, the design parameters β, and workspace positions γ. Symbol G represents the inequality constraint function that also depends on the design variables and parameters. Finally, α_l and α_u correspond to the lower and upper bounds of the design variables, respectively.

The optimization is performed over a wide design space, since the optimization problem possesses six design variables as depicted in Fig. 3 and explained in Table IV. Upper α_u and lower α_l limits on the design variables are imposed according to the statistical data on human finger and ergonomics considerations.

4.2. Solution methods

The multi-criteria optimization problem for the dimensional synthesis of the finger rehabilitation device is solved using the framework introduced in ref. [47, 48]. This optimization framework is based on Normal Boundary Intersection (NBI) method proposed by Das *et al.* [49] to efficiently obtain the Pareto-front curve characterizing the design trade offs. NBI method does not depend on the scales of the functions and yields a Pareto-front curve consisting of evenly distributed points. This method is computationally efficient thanks to fast gradient-based optimization techniques used for solving NBI subproblems. Computational performance of NBI is further increased by using solution of a subproblem to initialize the next subproblem. This method is more advantageous compared to weighted sum methods, since it also searches for the non-dominated solutions on the non-convex regions of the feasible domain.

https://doi.org/10.1017/S0263574714001957 Published online by Cambridge University Press

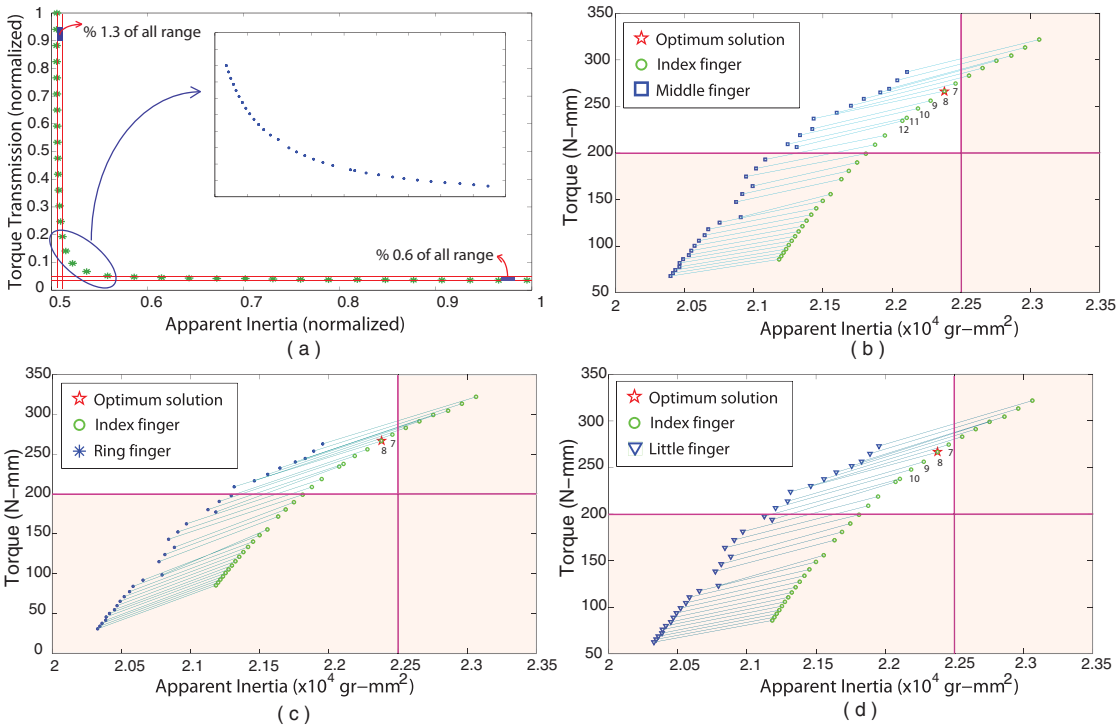

Fig. 4. (Colour online) (a) Pareto-front plot of the multi-criteria optimization problem and torque-inertia plots for the (b) middle finger, (c) ring finger and (d) little finger.

The single criterion optimum of each objective function, called shadow points, are required in order to initiate the NBI method. Since the objective functions are non-convex and possibly non-smooth, the shadow points are calculated using a global search method, called the culling algorithm.[50] Culling algorithm is an efficient form of brute force method for min-max optimization problems, since it performs independent searches in workspace and parameter-space, reducing the size of parameter-space after every workspace search. The algorithm works as follows: a global performance index is obtained by calculating the worst-case function value over the workspace for an initial parameter choice. For the workspace configuration where the global performance index is encountered, a parameter-space search is conducted. Then, the parameters that have a worse value than the current global performance index are eliminated from the parameter-space, since they are dominated. The second workspace search is performed for the parameter which has the best function value in the previous parameter-space search and algorithm continues by culling the search space both in the workspace and the parameter-space. Therefore, the search space is significantly reduced.

Since the performance of the culling algorithm is highly dependent on the discretization and our problem has a large design space, high discretization error might be attained. Therefore, after applying a coarse culling algorithm with a coarse discretization, a second culling search is performed with a finer discretization in a smaller search space around this solution. Finally, a pattern-search algorithm is performed utilizing the result obtained from the second finely discretized culling search.

4.3. Results of multi-criteria design optimization and selection of optimal device dimensions

The Pareto-front curve characterizing the trade-off between the kinematic efficiency of the mechanism and the apparent inertia over the workspace of the finger exoskeleton is presented in Fig. 4(a). All normalizations are performed by dividing by the largest value of the variable. From Fig. 4(a), one can observe that both objectives vary an important amount for different values of design variables of the finger exoskeleton. The trade-off between optimization criteria is low at the both ends of the plot, while there exits a significant trade-off in-between. The inset of Fig. 4(a) presents a close-up view of the high trade-off region, where a preferred solution is chosen.

All of the points on the Pareto-front curve represent non-dominated solutions of the multi-criteria optimization problem. A unique "optimal solution" can be selected from this set by considering the

https://doi.org/10.1017/S0263574714001957 Published online by Cambridge University Press

Table V. Worst-case and the average inertia and torque performance of the optimal design.

	DIP	PIP	MCP	Unit
Average torque	537	1178	869	[N-mm]
Worst case torque	262	777	488	[N-mm]
Activation torque[37]	200	290	290	[N-mm]
Worst case inertia	2.2×10^4	9.5×10^4	10.2×10^4	[gr-mm^2]
Average inertia	1.9×10^4	8.8×10^4	8.6×10^4	[gr-mm^2]
Average inertias in ref. [51]	5.3×10^4	9.6×10^4	21.7×10^4	[gr-mm^2]

primary objectives and introducing design thresholds on the performance requirements. To have a better intuition on the worst-case torque values of the optimization result, Jacobian is mapped into transmitted torque values. Thresholds on the performance requirements are introduced such that minimum worst-case torque is kept higher than 200 N-mm at the DIP joint, according to the torque required to activate the third knuckle of the finger as explained in Table III. Furthermore, an inertia threshold is set as 2.25×10^4 gr-mm^2 at DIP link in order to limit the number of feasible solutions.

These thresholds are decided such that the compromise solution assigns acceptable values for both of the objectives. In particular, a minimum torque requirement of 200 N-mm for the DIP joint ensures that adequate amount of torque is generated for all joints throughout the workspace. The inertia threshold is introduced to limit the number of optimal designs, by inspecting the non-dominated solutions on the Pareto-front curve. Being able to introduce performance thresholds as informed decisions, after carefully studying the optimal solution set and the trade-off between the competing design criteria is one of the main advantages of Pareto optimization techniques. *A priori* assignment of such thresholds, without first gaining an insight into the trade-off, is prohibitive.

The Pareto curve is formed for an average size index finger, since it is the most widely used and injured finger. However, ASSISTON-FINGER is designed for use with all fingers other than the thumb and the defined thresholds must also be satisfied by the middle, ring and little fingers. Figures 4(b)–(d) depict pairwise performance comparisons between middle, ring, little fingers vs the index finger, respectively. In these plots, the candidate solutions are determined as the ones that satisfy the thresholds for both fingers. After applying the thresholds to all fingers, the non-eliminated solutions are illustrated as points 7–12 in Fig. 4(b) for middle vs index finger, 7–8 in Fig. 4(c) for ring vs index finger and 7–10 in Fig. 4(d) for little vs index finger. Therefore, 7^{th} and 8^{th} points on the Pareto-front curve represent solutions that satisfy all constraints for all fingers. Considering the manufacturing tolerances, both of these solutions map to the optimal design variables of

$$\begin{aligned} x^* &= [L_1^* \quad L_2^* \quad L_{21}^* \quad L_{32}^* \quad L_4^* \quad \gamma_3^*]^T \\ &= [81\text{ mm} \quad 50\text{ mm} \quad 30\text{ mm} \quad 21\text{ mm} \quad 20\text{ mm} \quad 153^\circ]^T. \end{aligned}$$

Table V presents both the worst-case and the average inertia and torque levels for the optimal exoskeleton. The *continuous* torque outputs generated by ASSISTON-FINGER are adequate to overcome worst case gliding resistance encountered by the tendons reported as 1.23 ± 0.18 N in ref. [39] and to activate each knuckle of the finger.[37] The moving mass of the optimal ASSISTON-FINGER is less than 30 grams and its apparent inertia at each finger joint is significantly lower than that of similar devices in the literature. For comparison, the average apparent inertias calculated about DIP, MCP and PIP joints for a similar exoskeleton[51] are also reported in Table V. Note that the inertia values reported for ASSISTON-FINGER represent the apparent inertia of all moving parts calculated about the DIP, MCP and PIP joints, while the inertia values listed for[51] report inertia contributions of only the (single) closest phalanx of this exoskeleton.

Since the moving mass (due to gravitational forces) and the apparent inertia (due to accelerations) of an exoskeleton introduce undesired parasitic dynamics that interfere with the movement, the lowest possible values are targeted for better transparency of the device. The optimization process significantly improves the performance of the design according to both metrics. In particular, Table VI presents the performance of the optimal device together with the performance of our earlier prototype, that was designed without employing dimensional optimization. Optimal design

https://doi.org/10.1017/S0263574714001957 Published online by Cambridge University Press

Table VI. Performance comparison between optimal and ad-hoc designs.

	Torque	Apparent inertia
preliminary ad-hoc design	42 (N-mm)	5.1×10^4 (gr-mm^2)
optimal design	262 (N-mm)	2.2×10^4 (gr-mm^2)

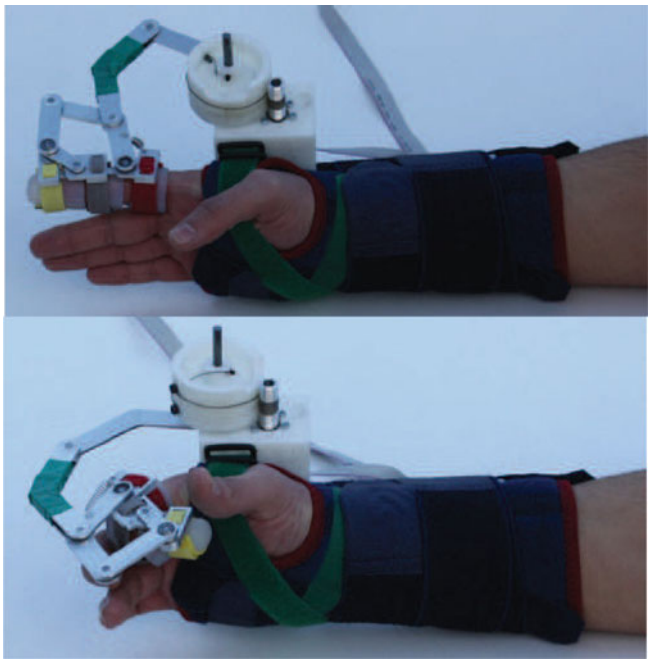

Fig. 5. (Colour online) ASSISTON-FINGER in extended (top) and flexed (bottom) configurations.

improves the apparent inertia of the design by two folds, while torque transmission is made four times more effective.

5. Implementation of ASSISTON-FINGER

The final design of the optimal ASSISTON-FINGER for tendon rehabilitation is presented in Fig. 5. In addition to using the link lengths/angles determined by optimal dimensional synthesis, the thickness of the finger exoskeleton is minimized to prevent collisions with the other fingers. The weight of the exoskeleton is kept low by using 6061 aluminum to fabricate the links and hard plastic to manufacture the grounded bracket and the capstan transmission. The overall device weighs 185 gr without the actuator. The weight of the device is distributed over the wrist and forearm using an adjustable splint. Weight of the device can further be distributed over the body by relocating the actuator away from the wrist. ASSISTON-FINGER is actuated by a capstan-driven direct drive DC motor equipped with an optical encoder. Potentiometers are instrumented at joints coinciding with PIP and DIP joints such that exact configuration of the finger can be measured at each instant of time.

Since the tension on the finger tendons directly depends on the position of the wrist,[52] we have implemented a manually adjustable wrist mount for the device. In particular, wrist is attached to device through straps, while its angle is adjusted by a hinge structure as shown in Fig. 6(a). Proper alignment of the exoskeleton to the proper finger is performed by coupling the exoskeleton to the drive shaft as shown in Fig. 6(b).

The attachment of exoskeleton to fingers needs to be fast and easy for comfort, while robustness of the mounting must be ensured for accurate measurements. Such an attachment is challenging for a finger exoskeleton, since there is not much space between fingers and the exoskeleton tied to one finger may cause discomfort to the neighboring finger. We have utilized snap fasteners as a practical

https://doi.org/10.1017/S0263574714001957 Published online by Cambridge University Press

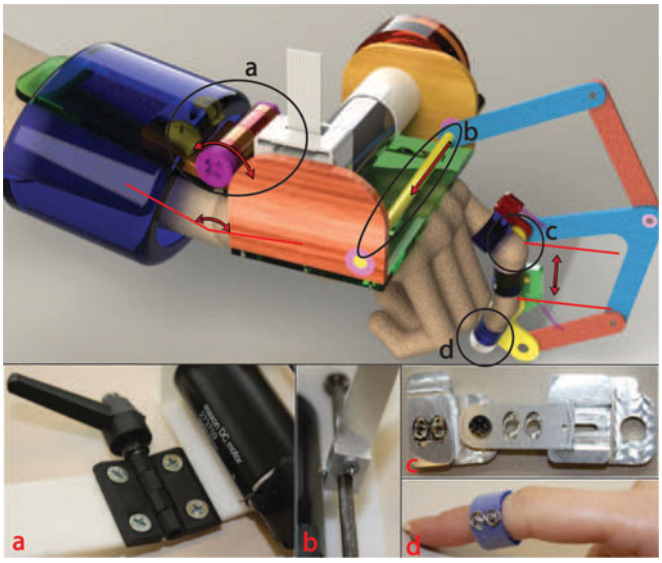

Fig. 6. (Colour online) Implementation details of ASSISTON-FINGER.

and low-profile means to attach a finger to the exoskeleton, within less than 2 min.[40] In particular, two snap fasteners are embedded to each knuckle, as shown in Figs. 6(c) and 6(d).

Ensuring alignment of exoskeleton axes with finger joint axes is crucial during therapies, since misalignments may cause discomfort, even injury under repetitive use. We ensure alignment of exoskeleton axes with finger joint axes by including human finger kinematics as an integral part of the underlying kinematics of the device and by employing passively adjustable links for each knuckle, as shown in Fig. 6(c), such that patients with different knuckle lengths can be accommodated. As a result, ASSISTON-FINGER is self-aligning and does not require any manual adjustments before its operation.

ASSISTON-FINGER is impedance controlled. Sensor measurements are input to a PC using an I/O card capable of 16 bit A/D conversion. The control torques for the finger exoskeleton are calculated in real-time and fed back to the device. A graphical user interface (GUI) displays the motion of the finger at 30 Hz during flexion and extension. The therapist can record the initial and final positions of the finger, determine the amount and direction of assistance/resistance, the number of repetitions, and the period of exercise via the GUI.

Interacting with human subjects requires a high level of safety. To prevent any harm or damage to patients, both software and hardware emergency systems have been implemented. As a safety precaution, ASSISTON-FINGER is designed to be passive back-driveable along each DoF, when the controllers are turned off. Passive back-driveability is ensured by direct-drive actuator driven capstan transmission with a low torque amplification ratio. Motor current limitations and diagnostics routines are also implemented in software, in addition to kill switches and emergency stops that are available at the interface. All mechanical components of the device have been rounded for safety.

Furthermore, since psychological factors are also important for the comfort of the patient and the therapist, throughout the therapy the device is placed such that both the patient and the therapist can observe the hand. Real objects are employed as task oriented end-effectors to promote psychological confidence of the patients.

6. Modes of Operation

Currently, ASSISTON-FINGER supports four different modes of tendon repair therapy: passive, active, active-assisted, and active-constrained modes. In the (patient) passive mode, the finger exoskeleton moves the injured finger on predetermined trajectories, while the patient remains passive. This mode is similar to the Duran technique used in conventional tendon therapy, where a therapist enforces coordinated motions to the injured finger within closely controlled joint limits, while the patient stays relaxed throughout the therapy. The (patient) active mode is used when active mobilization exercises

https://doi.org/10.1017/S0263574714001957 Published online by Cambridge University Press

are targeted. In this mode, the injured finger is active and the patient follows desired finger trajectories while the device is passive (or in an open-loop dynamics/friction compensation mode). This mode is similar to conventional tendon therapy, when the patient is required to perform active movements of flexion and extension exercises, but differs in that, the movements can be logged thanks to the device. In the active-assisted mode, the finger exoskeleton encourages the patient to stay active during extension (flexion), similar to the role of the assisting rubber band used in the Kleinert method. In contrast, in the active-constrained mode, the finger exoskeleton applies resistance to keep the patient passive during flexion (extension) of the injured finger, while the patient is active during extension (flexion). This mode can be used for strengthening exercises.

7. User Evaluations of ASSISTON-FINGER

A human subject experiment was conducted to quantify and compare the effect of ASSISTON-FINGER on the level of voluntary contraction of the muscles attached to the flexor tendons during active (patient driven) and passive (therapist or exoskeleton guided) exercises. It is hypothesized that during the exoskeleton driven mode, the voluntary contractions of the muscles and the tendon tension levels stay as low as the therapist guided exercises. It is also hypothesized that due to the parasitic dynamics of the device, the voluntary contraction levels for active patient motions with the device are higher than the levels without the device. One of the goals of this experiment is to obtain a quantifiable measure of device interference during active motions, such that the need for active dynamics compensation can be justified.

7.1. Participants

Four volunteers (2 males, 2 females, ages 23–28, all right-handed), all graduate students in engineering, participated in the experiment. All volunteers reported a high level of physical activity and were free of any musculoskeletal, cardiac, pulmonary and metabolic disorders. The participants were given extra credit in an engineering class upon completion of the experiment. All participants signed consent forms approved by the IRB of Sabancı University to allow human performance data to be obtained and analyzed.

7.2. Task

The task was selected as the repetitive flexion/extension motion of the index finger throughout the range of the MCP joint, with a period of six seconds. Participants were instructed to stay relaxed and perform smooth motions, while trying to synchronize with the period of the reference signal. Visual and auditory reference signal were displayed during the experiment to guide participants with the timing of the task, however, strict timing was not enforced.

7.3. Experiment setup

The setup consisted of a desktop computer, a monitor screen, a wristband, an sEMG data acquisition device and the under-actuated force feedback finger exoskeleton, ASSISTON-FINGER. Volunteers sat in front of the monitor screen with the index fingers of their dominant hands firmly attached to the exoskeleton. The elbows of the participants were supported to obtain a natural and comfortable posture. To ensure a robust and repeatable coupling between the finger and the exoskeleton, a wristband was tightly wrapped around the wrist in order to stabilize its movement at a constant angle of 20°. Then, the base platform of the exoskeleton was tied over the wrist via bandage straps and the transverse location of the finger exoskeleton was adjusted on the driver shaft to accommodate the natural finger motions. To maximize comfort and hygiene, each phalanx of index finger was covered with a silicon ring before being attached to the exoskeleton using Vectro straps. The joint axes of the exoskeleton mechanism naturally adapts to the rotation of finger joints thanks to sliders embedded into the linkage design. Figure 7 illustrates a volunteer coupled to ASSISTON-FINGER.

sEMG signals were recorded by a custom build data acquisition device. Electrical noises and motion artifacts in the raw sEMG data were suppressed by a fourth order active band-pass filter with pass band of 20–500 Hz. An instrumentation amplifier with a gain of 1000 was employed to amplify the low amplitude voltage level of sEMG signal. The A/D conversion is executed with a 16 bit ADC card. The sampling rate was set to 1 kHz.

https://doi.org/10.1017/S0263574714001957 Published online by Cambridge University Press

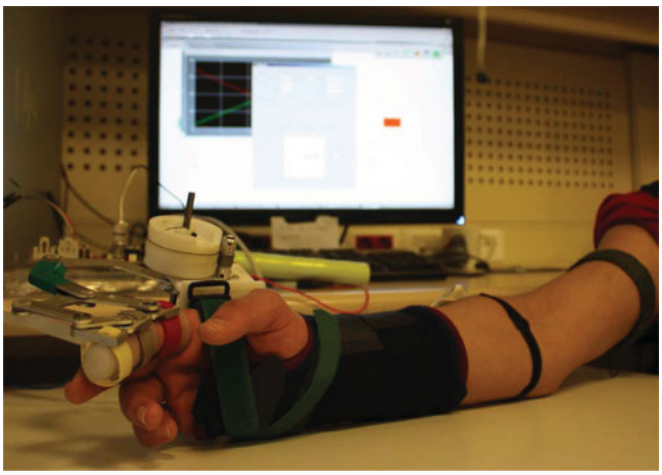

Fig. 7. (Colour online) A volunteer attached to ASSISTON-FINGER.

7.4. Experiment protocol

The experiment included four sessions: active (A), active with finger exoskeleton (F), human guided passive (H), and exoskeleton driven passive (E). Each session consisted of six subsessions, each subsession contained 10 trials, with each trial lasting for about 6 s. The subsessions were separated by 2–3 min breaks, such that a session was completed in less than 30 min. Each volunteer took place in all of the experiment subsessions. The order of the sessions was randomly assigned to each participant. Before the experiment, each participant was given up to 5 min. to become familiar with the finger exoskeleton and the task.

The active (A) trials served as the control set for the active with finger exoskeleton (F) trials, while the human guided passive (H) trials were the control set for the exoskeleton driven passive (E) trials. During the exoskeleton driven (E) trials, the actuators of the device provided guidance forces, while during the human guided passive (H) trials, the participants imposed the motion of the finger using their other hands.

Before the experiment, first a skin preparation step was administrated, followed by the positioning of the pairs of sEMG electrodes with an inter-electrode distance of 2 cm over the belly of the extensor digitorum communis (EDC) and extensor indicis proprius (EIP) muscles, which are responsible for the motion of index finger.[53]

7.5. Performance measures

To evaluate the feasibility and applicability of ASSISTON-FINGER for tendon repair therapies, two task performance measures were analyzed during the flexion movement of the finger: (1) average muscle activation measured through the average of the root mean square (RMS) of sEMG signals and (2) the maximum tendon tension estimated through a biomechanical finger model. In particular, the average muscle activation serves as a quantitative metric to evaluate the beneficial (parasitic) effect of exoskeleton in lowering (increasing) muscle recruitment levels during patient passive (active) tendon therapy exercises, while the estimates of the maximum of tendon tension levels are useful in evaluating the level of safety of the device in delivering tendon therapies.

7.5.1. Average muscle activation. The average muscle activation levels were calculated to evaluate efficacy of the assistance provided by the exoskeleton when the volunteers were passive, and the level of parasitic dynamics induced by the device when the volunteers were active.

Since sEMG signals are superpositions of the electrical potentials generated by motor units, the amplitude of sEMG signals is associated with the motor unit activities.[54] In the literature, the RMS value of an sEMG signal that reveals its mean power in the time domain, has been proposed as a reliable measure of the force contribution of the relevant muscle group.[55]

The RMS values of sEMG signals were calculated for intervals of 60 s, during which the muscles went through both the flexion and extension phases. Envelopes of the rectified sEMG signals were calculated by post processing the rectified sEMG signals with a 250 Hz FIR filter. In order to

https://doi.org/10.1017/S0263574714001957 Published online by Cambridge University Press

control for individual differences in the task performance, each participant was asked to perform an evaluation session. The purpose of the evaluation session was to measure the resting and the maximum voluntary contraction thresholds of each participant, so that the experiment data could be normalized. The envelopes were post-processed by subtracting resting potential offsets determined for each subject during the evaluation experiment. To locate the onset and offset time of muscle extensions on the rectified sEMG signals, the signals were convolved with their envelopes. Finally, the percent voluntary contractions were calculated by normalizing the mean RMS of the sEMG signal by the mean RMS value pertaining to maximum voluntary contraction.

7.5.2. Maximum tendon tension. To evaluate safety of ASSISTON-FINGER against gap formation or rupture of the repair site, it is necessary to compare tendon tension levels of exoskeleton assisted therapies with those of the conventional exercises. Unfortunately, the use of invasive *in vivo* tendon tension measurements is infeasible during tendon repair therapies or for device evaluations.

Experimental evidence in ref. [2, 52, 56] suggests that the tendon tension is a complex function of the joint positions, the wrist orientation, the external finger tip forces and the flexor/extensor muscle activities. Along these lines, many biomechanical models of the finger have been developed in the literature to estimate tendon tensions.[57–61] In this study, we utilize sEMG-based tendon tension estimation method covered in ref. [59, 61]. This method is based on a linear relationship between sEMG and tension within a muscle[38,62] and can provide tendon tension estimates for extrinsic muscles, for which sEMG signals are available. According to this model, the tendon tensions t are calculated from the product of the physiological cross-sectional area (PCSA) of the muscle, the maximum isometric muscle stress (σ_{max}) and the muscle activation level (e) as

$$t = PCSA \cdot \sigma_{max} \cdot e \tag{15}$$

In our experiments, the wrist orientation was fixed at 20°, while no external finger tip forces were applied. sEMG measurements were taken from extensor digitorum communis (EDC) and extensor indicis proprius (EIP) muscles and σ_{max} and PCSA were set to 0.35 N/mm^2 and 250 mm^2, respectively.[63] Finally, the maximum muscle activation levels e_{max} were determined from the percent voluntary contractions as detailed in the previous subsection.

It is important to emphasize here that, even though the use of biomedical models is justified to guide biomechanics studies and device evaluations, these estimates cannot be considered reliable and accurate enough for medical evaluations. For instance, two established biomechanical models of the finger have been compared in terms of tendon tension estimates in ref. [64], and differences of about 80% were reported for extensor tension estimates between the models. Besides, biomechanical models developed for healthy humans are not recommended for estimating tension levels after tendon repair. In addition to the strength of the suture material and type of the knot, the quality of the surrounding tissue, *unique to each patient*, affect the holding capacity of the suture within the tendon.[39,65]

8. Results and Discussion

During the experiment, the sEMG signals responsible for finger extension were recorded from the extensor digitorum communis (EDC) and extensor indicis proprius (EIP) muscles. Note that, in addition to firing during extension movement of the finger, the extensor muscles also produce sEMG signals when their neighbouring and/or antagonistic muscle groups are active. Since the repetitive task of the flexion and extension the index finger requires the collaboration of antagonistic muscle groups, the recorded signals need to be processed to extract sEMG signals produced during the finger extension, especially for the sessions H and E, which feature low muscle activation levels. At the first step, the rectified sEMG signals were enveloped and their offsets were extracted. Secondly, the sEMG signals were convoluted with their envelopes to extract the relevant sEMG signals that were generated during finger extension. Finally, the overlaps of the envelope of the convolutions with the rectified sEMG signals were used to extract the onset and final time of muscle activations. Figure 8 presents typical sEMG data collected from a participant during all four conditions and the signal processing steps applied to this data. In particular, in the top row of the figure, the dashed green lines present the finger joint angles measured by the device encoders (available only for trials with the exoskeleton), red lines represent the rectified sEMG signals, while blue signals depict the envelope of

https://doi.org/10.1017/S0263574714001957 Published online by Cambridge University Press

Table VII. Summary of significance measured by ANOVA for average RMS values.

Effect	Significance
Guidance	$F(3, 12) = 6.32,\ p < 0.01^*$
Subsession	$F(5, 60) = 1.64,\ p > 0.05$
Interaction	$F(15, 60) = 1.26,\ p > 0.05$

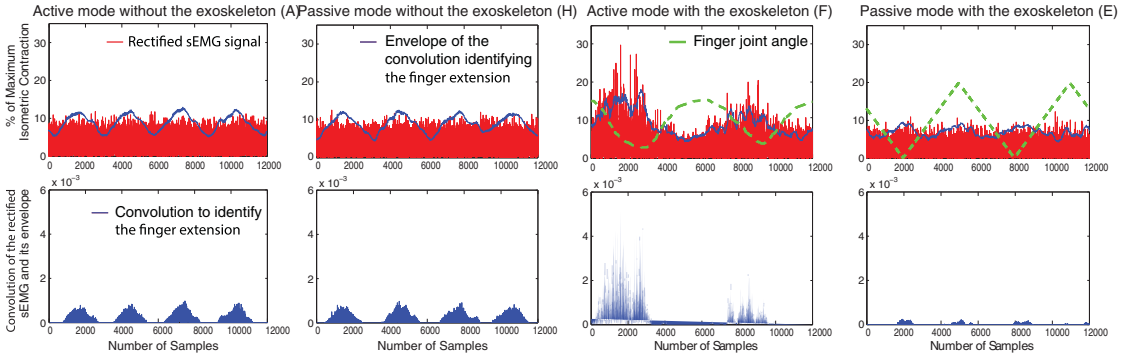

Fig. 8. (Colour online) Typical data of the participants during all four conditions.

extension motion extracted from the convolutions. In the bottom row of the figure, the convolutions of the rectified sEMG signals with their envelopes are presented.

Since the experiment consisted of two factors, namely the guidance mode and subsessions, a repeated measures ANOVA is utilized to verify the tested hypotheses. The guidance mode is analyzed between-subjects, with four levels of active without the exoskeleton (A), active with the exoskeleton (F), passive without the exoskeleton (human guided) (H), and passive with the exoskeleton (exoskeleton driven) (E). Six subsessions are analyzed as a within-subject factor.

A summary of ANOVA results over the average muscle activation metric is listed in Table VII. The results reveal a significant main effect of guidance and no significant effects of subsession or interaction.

Dependent-measures t-tests are conducted to compare guidance modes. Muscle activation levels between H and E, E and A, and A and H guidance modes are found to be not statistically significant. However, the muscle activation levels of E mode are significantly lower than F mode ($F(1,6) = 8.01$, $p < 0.05$), H mode are significantly lower than F mode ($F(1,6) = 6.13$, $p < 0.05$), and A mode are significantly lower than F mode ($F(1,6) = 5.62$, $p < 0.05$). The box plot characterizing the average muscle activation levels is presented in Fig. 9.

The statistical results on the average muscle activation levels indicate that exoskeleton driven mode (E) is as effective as therapist guided (H) exercises in reducing muscle activation levels. This is an encouraging result, supporting appropriateness of the device for clinical use during early repair therapy. The muscle activation levels of active (A) and passive (H) movements without the device are found to be similar, as also reported in the literature.[2] The muscle recruitment in active movement with the device (F) is significantly higher than active movements without the device (A). This result indicates that even with 30 grams of moving inertia and very low apparent inertia, when not actuated, the device dynamics interfere with the natural motion of the finger. Hence, in order not to interfere with finger movements, finger exoskeletons also need to target active back-driveability, by always engaging their controllers with active dynamics compensation. Similarly, caution must be exercised by the therapists to ensure that early tendon therapy patients are attached to the device always after the device controllers are engaged.

Table VIII presents repeated measure ANOVA results over the maximum tendon tension metric, while the box plot characterizing the maximum tension levels is presented in Fig. 10. Note that the tendon tension estimates are in good agreement with the *in vivo* tension measurements reported in the literature.[66]

https://doi.org/10.1017/S0263574714001957 Published online by Cambridge University Press

Table VIII. Summary of significance measured by ANOVA for the maximum tendon tension estimates.

Effect	Significance
Guidance	$F(3, 12) = 4.01,\ p < 0.05^*$
Subsession	$F(5, 60) = 1.60,\ p > 0.05$
Interaction	$F(15, 60) = 0.91,\ p > 0.05$

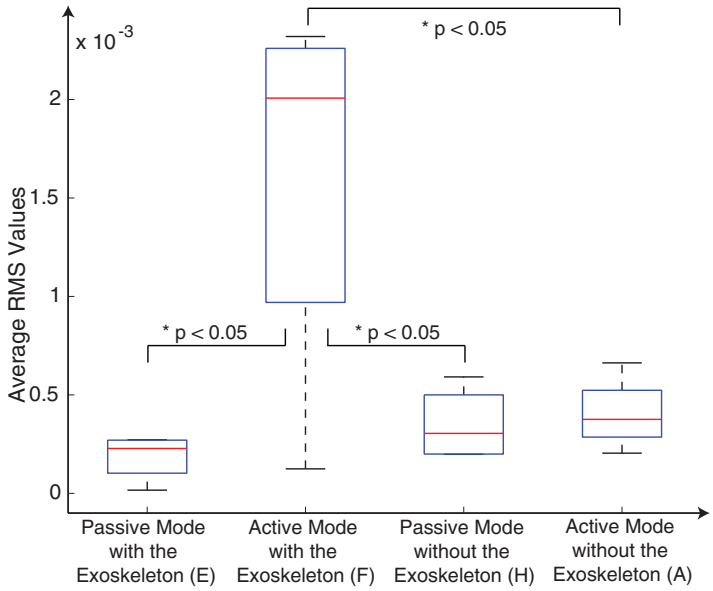

Fig. 9. (Colour online) Box plot of the average RMS of sEMG signals.

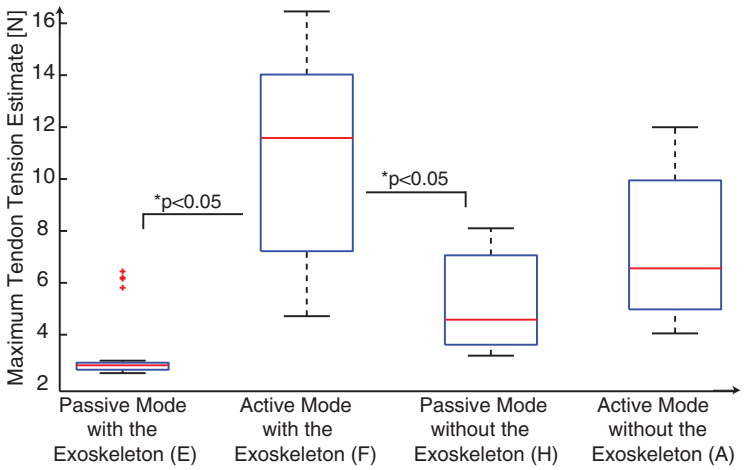

Fig. 10. (Colour online) Box plot of the maximum tendon tension estimates.

Once again, ANOVA results reveal a significant main effect of guidance and no significant effects of subsession or interaction. Dependent-measures t-tests are conducted to compare guidance modes. The maximum tendon tensions between E and F guidance modes and H and F guidance modes are found to be statistically significant at $p < 0.05$ level, while all other pairs are found to be not significant. In particular, the maximum tendon tension level of E mode is significantly lower than F mode ($F(1,6) = 11.07$, $p < 0.05$), and H mode is significantly lower than F mode ($F(1,6) = 5.85$, $p < 0.05$). These statistical results on the maximum tendon tension levels indicate that exoskeleton driven mode (E) is as effective as the therapist guided (H) exercises in helping to keep the maximum tendon

https://doi.org/10.1017/S0263574714001957 Published online by Cambridge University Press

tension levels low. Once again, the maximum tendon tension levels of active (A) and passive (H) movements without the device are found to be not significantly different as reported in the literature.[2] The maximum tendon tension levels in active movement with the device (F) is also not significantly higher than active movements without the device (A). This result is sensible, since unlike the average muscle activation metric, the maximum tendon tension metric is an instantaneous worst case measure and even though average muscle activation levels are increased since more work has to be done due to the parasitic dynamics of the device, the peak tension levels can remain at similar levels. Both results comparing exoskeleton driven mode (E) with the therapist guided mode (H) and active movement with the device mode (F) with active movements without the device mode (A) provide empirical evidence that the use of the device is safe, since maximum tendon tension levels are kept as low as conventional therapy case when the device is used.

9. Conclusions

We have presented ASSISTON-FINGER, an under-actuated finger exoskeleton designed to assist flexion/extension motions of the finger within its full range, in a natural and coordinated manner, while helping to keep the tendon tension within acceptable limits. We have introduced kinematics of ASSISTON-FINGER, presented its optimal dimensional synthesis with respect to multiple performance criteria and provided implementation details. We have also provided results of feasibility studies on healthy volunteers and showed the efficacy of exoskeleton driven exercises on keeping the muscle recruitment and the maximum tendon tension levels as low as human guided exercises.

Our future works include larger scale human subject experiments and case studies with patients suffering from tendon injuries. Since the exoskeleton can simultaneously measure finger movements, robot actuation forces, and muscle activation levels, utilizing these measurements to provide quantitative measures of recovery and to guide physical therapy programs is also part of our future work.

Acknowledgments

This work has been partially supported by TUBITAK Grant 111M186. Authors would like to thank Duygun Erol Barkana from Yeditepe University and Dr. Halil Bekler from Yeditepe Hospital and anonymous reviewers for their valuable comments and suggestions.

References

1. C. A. Trombly, "Occupational therapy for physical dysfunction," *Stroke*, 454–471 (1989).
2. J. T. Dennerlein, "Finger flexor tendon forces are a complex function of finger joint motions and fingertip forces," *J. Hand therapy* **18**, 120–127 (2005).
3. J. W. Strickland and S. V. Glogovac, "Digital function following flexor tendon repair in zone II: A comparison of immobilization and controlled passive motion techniques," *J. Hand Surg.* **5A**, 537–543 (1980).
4. T. Tanaka, P. C. Amadio, C. Zhao, M. E. Zobitz and K. N. An, "Flexor digitorum profundus tendon tension during finger manipulation," *J. Hand Theraphy* **18**, 330–338 (2005).
5. G. V. Strien, "Postoperative management of flexor tendon injuries," *Rehabil. Hand* **1**, 390–409 (1990).
6. K. M. Stewart, "Concepts in hand rehabilitation," *Tendon Injuries* 353–392 (1992).
7. C. D. Kerr and J. R. Burczak, "Dynamic traction after extensor tendon repair in zones 6, 7 and 8: A retrospective study," *J. Hand Surg.* **14B**, 21–22 (1989).
8. R. B. Evans, "Clinical application of controlled stress to the healing extensor tendon: A review of 112 cases," *Phys. Theraphy* **69**, 1041–1049 (1989).
9. J. W. Strickland, "Flexor tendon repair," *Hand Clinics* **1**, 55–68 (1985).
10. M. N. Halikis, P. R. Manske, H. Kubota and M. Aoki, "Effect of immobilization, immediate mobilization, and delayed mobilization on the resistance to digital flexion using a tendon injury model," *J. Hand Surg.* **22**, 464–472 (1997).
11. K. W. Cullen, P. Tolhurst and P. R. E. Lang, "Flexor tendon repair in zone 2 followed by controlled active mobilisation," *J. Hand Surg.* **14B**, 392–395 (1989).
12. H. E. Kleinert, S. Schepel and T. Gill, "Flexor tendon injuries," *Surg. Clin. North Am.* **61**, 267–286, (1981).
13. G. B. Prange, M. J. Jannink, C. G. Groothuis-Oudshoorn, H. J. Hermens and M. J. Ijzerman, "Systematic review of the effect of robot-aided therapy on recovery of the hemiparetic arm after stroke," *J. Rehabil. Res. Dev.* **43**(2), 171–184 (2006).
14. G. Kwakkel, B. J. Kollen and H. I. Krebs, "Effects of robot-assisted therapy on upper limb recovery after stroke: A systematic review," *Neurorehabilitation and Neural Repair* **22**(2), 111–121 (2008).

15. J. Mehrholz, T. Platz, J. Kugler and M. Pohl, "Electromechanical and robot-assisted arm training for improving arm function and activities of daily living after stroke," *Stroke* **40** (2009).
16. K. Nykanen, The Effectiveness of Robot-Aided Upper Limb Therapy in Stroke Rehabilitation: A Systematic Review of Randomized Controlled Studies *Master's Thesis* (University of Jyvskyl, Institute of Health Sciences, Physiotherapy, 2010).
17. "Theraband website," `http://www.thera-band.com/store/products.php?ProductID=22`.
18. "Gripmaster website," `http://www.gripmaster.com.au/index1.htm`.
19. "VQ Orthocare website," `http://www.jimmedical.com/products/8091-portable-hand-cpm`.
20. "Tyromotion website," `http://www.tyromotion.com/`.
21. H. Kawasaki, "Multi-fingered haptic interface robot and its application systems," *Solid State Phenom.* **144**, 1–8 (2009).
22. P. Stergiopoulos, P. Fuchs and C. Laurgeau, "Design of a 2-finger hand exoskeleton for VR grasping simulation," *EuroHaptics* (2003).
23. A. Frisoli, F. Salsedo, M. Bergamasco and B. R. M. C. Carboncini, "A force-feedback exoskeleton for upper-limb rehabilitation in virtual reality," *Appl. Bionics Biomech.* **6**, 115–126 (2009).
24. M. Mulas, M.Folgheraiter and G. A. Gini, "EMG-controlled Exoskeleton for Hand Rehabilitation," *Proceedings of the IEEE International Conference on Rehabilitation Robotics* (2005) pp. 371–374.
25. T. Worsnopp, M. Peshkin, J. Colgate and D. Kamper, "An Actuated Finger Exoskeleton for Hand Rehabilitation following Stroke," *Proceedings of the IEEE International Conference on Rehabilitation Robotics* (Jun. 2007) pp. 896–901.
26. S. V. Adamovich, G. G. Fluet, A. Mathai, Q. Qiu, J. Lewis and A. S. Merians, "Design of a complex virtual reality simulation to train finger motion for persons with hemiparesis: A proof of concept study," *J. NeuroEngineering Rehabil.* **6**(1), 1–13 (2009).
27. D. Jack, R. Boian, A. S. Merians, M. Tremaine, G. C. Burdea and S. V. Adamovich, "Virtual reality-enhanced stroke rehabilitation," *IEEE Trans. Neural Syst. Rehabil. Eng.* **9**, 308–318 (2001).
28. C. A. Avizanno, F. Barbagli, A. Frisoli and M. Bergamasco, "The Hand Force Feedback: Analysis and Control of a Haptic Device for the Human Hand," *Proceedings of the IEEE International Conference on Systems, Man and Cybernetics* (2000) pp. 989–994.
29. A. Wege and G. Hommel, "Development and Control of a Hand Exoskeleton for Rehabilitation of Hand Injuries," *Proceedings of the International Conference on Intelligent Robots and Systems* (2005) pp. 3046–3051.
30. U. Mali and M. Munih, "HIFE-haptic interface for finger exercise," *IEEE/ASME Trans Mechatronics* **11**, 93–102 (2006).
31. Y. Fu, P. Wang, S. Wang, H. Liu and F. Zhang, "Design and Development of a Portable Exoskeleton based cpm Machine for Rehabilitation of Hand Injuries," *Proceedings of the IEEE International Conference on Robotics and Biomimetics* (Dec. 2007) pp. 1476–1481.
32. Y. Fu, P. Wang and S. Wang, "Development of a Multi-DoF Exoskeleton Based Machine for Injured Fingers," *IEEE International Conference on Intelligent Robots and Systems* (Sep. 2008) pp. 1946–1951.
33. I. H. Ertas, E. Hocaoglu, D. E. Barkana and V. Patoglu, "Finger Exoskeleton for Treatment of Tendon Injuries," *Proceedings of the IEEE International Conference on Rehabilitation Robotics* (2009).
34. P. S. Lum, S. Mulroy, R. L. Amdur, P. Requejo, B. I. Prilutsky and A. W. Dromerick, "Gains in upper extremity function after stroke via recovery or compensation: Potential differential effects on amount of real-world limb use," *Top. Stroke Rehabil.* **16**(4), 237–253 (2009).
35. J. C. Becker and N. V. Thakor, "A study of the range of motion of human fingers with application to anthropomorphic designs," *IEEE Trans. Biomed. Eng.* **35**, 110–117 (1988).
36. B. Alexander and K. Viktor, "Proportions of hand segments," *Int. J. Morphology* **8**(3), 755–758 (2010).
37. T. Mouri, H. Kawasaki, Y. Nishimoto, T. Aoki, Y. Ishigure and M. Tanahashi, "Robot hand imitating disabled person for education/training of rehabilitation," *J. Robot. Mechatronics* **20**(2), 280–288 (2008).
38. F. J. Valero-Cuevas, F. E. Zajac and C. G. Burgar, "Large index finger tip forces are produced by subject-independent patterns of muscle excitation," *J. Biomech.* **31**, 693–703 (1998).
39. T. Tanaka, P. C. Amadio, C. Zhao, M. E. Zobitx, C. Yang and K.-N. An, "Gliding characteristics and gap formation for locking and grasping tendon repairs: A biomechanical study in a human cadaver model," *J. Hand Surg.* **29A**(1), 6–14 (2004).
40. V. Patoglu, G. Ertek, O. Oz, D. Zoroglu and G. Kremer, "Design Requirements for a Finger Rehabilitation Robot: Results from a Survey of Engineers and Health Professionals," *Proceedings of the ASME International Design Engineering Technical Conferences & Computers and Information in Engineering Conference IDETC/CIE* (2010).
41. L. Birglen, T. Laliberte and C. Gosselin, *Underactuated Robotic Hands* (Springer, Berlin, 2008).
42. R. Cabas, L. M. Cabas and C. Balaguer, "Optimized Design of the Underactuated Robotic Hand," *Proceedings of the International Conference on Robotics and Automation* (May, 2006), pp. 982–987.
43. S. M. Nacy, S. S. Hassan and S. H. Bakhy, "Geometric optimization of three-phalanx prosthesis underactuated fingers using particles swarm algorithm," *Am. J. Eng. Appl. Sci.* **2**(2), 381–387 (2009).
44. L. C. Wu, G. Carbone and M. Ceccarelli, "Designing an underactuated mechanism for a 1 active dof finger operation," *Mech. Mach. Theory* **44**(2), 336–348 (Feb. 2009).

45. S. Yao, M. Ceccarelli, G. Carbone and Z. Lu, "An Optimal Design for a New Underactuated Finger Mechanism," *The Second European Conference on Mechanism Science* (2008) pp. 149–157.
46. L. Birglen and C. Gosselin, "Optimal design of 2-phalanx underactuated fingers," (2004) pp. 110–116.
47. R. Unal, G. Kiziltas and V. Patoglu, "A Multi-criteria Design Optimization Framework for Haptic Interfaces," *Proceedings of the Symposium on Haptic Interfaces for Virtual Environment and Teleoperator Systems* (Mar. 2008) 231–238.
48. R. Unal, G. Kiziltas and V. Patoglu, "Multi-criteria Design Optimization of Parallel Robots," *Proceedings of the IEEE Conference on Robotics, Automation and Mechatronics* (Sep. 2008) pp. 112–118.
49. I. Das and J. E. Dennis, "Normal-boundary intersection: A new method for generating the pareto surface in nonlinear multi-criteria optimization problems," *SIAM J. Optim.* **8**(3), 631–657 (1998).
50. L. Stocco, S. E. Salcudean and F. Sassani, "Fast constrained global minimax optimization of robot parameters," *Robotica* **16**(6), 595–605 (1998).
51. Li Jiting, Wand Shuang, W., Zheng Ruoyin, Zhang Yuru and Chen Zhongyuan, "Development of a hand exoskeleton system for index finger rehabilitation," *Chin. J. Mech. Eng.* **24**(5), 215–224 (2011).
52. K. Kursa, L. Lattanza, E. Diao and D. Rempel, "*In vivo* flexor tendon forces increase with finger and wrist flexion during active finger flexion and extension," *J Orthopaedic Res.* **24**, 763–769 (2006).
53. C. J. DeLuca, "The use of surface electromyography in biomechanics," *J. Appl. Biomech.* **13**, 135–163 (1997).
54. D. Farina, R. Merletti and M. R. Enoka, "The extraction of neural strategies from the surface EMG," *J. Appl. Physiol.* **96**, 1486–1495 (2004).
55. J. Kollmitzer, R. G. Ebenbichler and A. Kopf, "Reliability of surface electromyographic measurements," *Clin. Neurophysiol.* **110**, 725–734 (1999).
56. E. S. Powell and I. A. Trail, "Forces transmitted along human flexor tendons - The effect of extending the fingers against the resistance provided by rubber bands," *J. Hand Surg.* 1–4 (2009).
57. J. L. Sancho-Bru, A. Perez-Gonzalez, M. Vergara-Monedero and D. Giurintano, "3D dynamic model of human finger for studying free movements," *J. Biomech.* **34**, 1491–1500 (2001).
58. N. S. Pollard and R. C. Gilbert, "Tendon Arrangement and Muscle Force Requirements for Humanlike Force Capabilities in a Robotic Finger," *Proceedings of the IEEE International Conference on Rehabilitation Robotics* (2002) pp. 3755–3762.
59. L. Vigouroux, F. Quaine, A. Labarre-Vila and F. Moutet, "Estimation of finger muscle tendon tensions and pulley forces during specific sport-climbing grip techniques," *J. Biomech.* **39**, 2583–2592 (2006).
60. F. J. Valero-Cuevas, J. W. Yi, D. Brown, R. V. McNamara, C. Paul and H. Lipson, "The tendon network of the fingers performs anatomical computation at a macroscopic scale," *IEEE Trans. Biomed. Eng.* **54**, 1161–1166 (2007).
61. L. Vigouroux, F. Quaine, A. Labarre-Vila, D. Amarantini and F. Moutet, "Using EMG data to constrain optimization procedure improves finger tendon tension estimations during static fingertip force production," *J. Biomech.* **40**, 2846–2856 (2007).
62. C. Long and M. E. Brown, "Electromyographic kinesiology of the hand. Muscles moving the long finger," *J. Bone Joint Surg.* **46**, 1683–1706 (1964).
63. V. R. Preedy (ed.), *Handbook of Anthropometry: Physical Measures of Human Form in Health and Disease* (Springer, New York, 2012).
64. O. Warlow and S. Lawson, "Factors Influencing Calculated Tendon Tensions in Two Established Phalangeal Models," **In**: *Computer Methods in Biomechanics and Biomedical Engineering* (2010).
65. J. Maquirriain, "Achilles tendon rupture: Avoiding tendon lengthening during surgical repair and rehabilitation," *Yale J. Biol. Med.* **84**(3), 289–300 (2011).
66. J. T. Dennerlein, E. Diao, C. D. Mote and D. M. Rempel, "*In vivo* finger flexor tendon force while tapping on a keyswitch," *J. Orthopaedic Res.* **17**, 178–184 (1999).